Research Square

Preprints are preliminary reports that have not undergone peer review.
They should not be considered conclusive, used to inform clinical practice,
or referenced by the media as validated information.

Synthesis and characterization of 2-methylimidazole end capped Zwitter ion functionalized Polyaniline

R. Anbarasan

anbu_may3@yahoo.co.in

Saveetha University

A. Thamizhlarasan

Madras Institute of Technology (MIT)

A. B. Thamizhlthendral

Saveetha Engineering College

B. Meenarathi

Saveetha University

Research Article

Keywords: PANI. Chain end capping. FC alkylation. Zwitter ion formation

Posted Date: June 17th, 2026

DOI: https://doi.org/10.21203/rs.3.rs-9608622/v1

License: This work is licensed under a Creative Commons Attribution 4.0 International License.
Read Full License

Additional Declarations: No competing interests reported.

Synthesis and characterization of 2-methylimidazole end capped Zwitter ion functionalized Polyaniline

R. Anbarasan[1] · A. Thamizhlarasan[2] · A. Thamizhlthendral[3] · B. Meenarathi[1]

[1]Department of Product Development, SIMATS-Engineering, Saveetha University, Thandalam – 602 105, Tamilnadu, India,

[2]Department of Plastics and Rubber Technology, Madras Institute of Technology (MIT), Chromepet, Chennai, 600 044, Tamilnadu, India,

[3]Department of Chemical Engineering, Saveetha Engineering College, Thandalam – 602 105, Tamilnadu, India.

---

* Corresponding author
E-mail address: anbu_may3@yahoo.co.in

Abstract
Due to the lack of functional groups, the processability of polyanilines (PANIs) are limited. Poor solubility in common solvents, high rigidity and hydrophobicity are the important problems associated with PANI. To enhance its processability, acid and amine groups were grafted onto the PANI backbone via a Friedel-Crafts (FC) alkylation reaction, carried out at 85 °C for 6 hours under a nitrogen atmosphere with vigorous stirring. Prior to this, the PANI backbone was synthesized through free radical (FR) solution polymerization, initiated by peroxy disulphate (PDS), using aniline monomer at 0–5 °C under nitrogen purging. A key modification during synthesis was the inclusion of *2*-methylimidazole (*2*MI), which imparted hydrophilicity and facilitated end-capping of the polymer chains. The functionalized PANIs were thoroughly characterized by various analytical tools, antimicrobial properties and thermal properties. Following acid functionalization, the water contact angle (WCA) increased to 61.4°, attributed to the formation of Zwitter ionic structures, as evidenced by an FTIR peak at 1640 cm^{-1}. This modification also significantly improved the water solubility of PANI. The % yield of A3 sample was found to be low due to the availability of few reaction cite on the aromatic ring of PANI for second grafting reaction. A plausible reaction mechanism was proposed based on the experimental findings, which were carefully analyzed and compared with values reported in the literature.

Keywords: PANI · Chain end capping · FC alkylation · Zwitter ion formation

Introduction
The applications of conducting polymers across various scientific and engineering domains are expanding rapidly, primarily due to their high electrical conductivity and ease of synthesis. Additionally, their electrochromic properties further broaden their range of potential uses. Despite these advantages, conducting polymers like polyaniline (PANI) face several technical challenges, including hydrophobicity, high rigidity, and poor solubility in water and other solvents [1]. These limitations have been critically examined and are primarily attributed to the absence of functional groups, which hinders their interaction with solvents and compatibility with other polymer systems. Attempts to polymerize functionalized aniline monomers have shown reduced polymerization rates and low yields due to steric hindrance. Moreover, post-polymerization functionalization, while offering better control, often results in reduced electrical conductivity values. A further complication is the low molecular weight of the resulting conducting polymers [2]. In light of these issues, the present research is focused on the synthesis of water-processable PANI with enhanced electrical conductivity through a carefully designed post-functionalization strategy.

To address the challenges associated with PANI processability, an extensive literature review was conducted to evaluate the various strategies employed by researchers. In 2025, Kishnani et al synthesized PANI for non-enzymatic lactic acid detection, reporting a glass transition temperature (T_g) between 30 and 40 °C [3]. The MOF modified PANI was prepared and its electro-rheological behaviour was studied [4]. Another method involved incorporating functionalized graphene oxide to improve processability [5], while functionalized single-walled carbon nanotube (SWCNT)-doped PANI was developed for photocatalytic applications [6]. PANI functionalized with various groups was confirmed through FTIR and UV-visible spectroscopy [7]. Hydrogen peroxide-initiated polymerization of aniline yielded a highly porous PANI structure [8], and reduced graphene oxide (GO)-functionalized PANI was explored for transistor applications [9]. Metal oxide-functionalized PANI demonstrated excellent electrical conductivity [10], and doping with specific agents also improved PANI's

processability [11]. Blending techniques have proven to be simple yet effective in achieving similar improvements.

Nikolaidis et al employed a co-polymerization approach to enhance processability [12], while Tritscher et al developed surfactant-doped PANI for fuel cell applications [13]. For various end-use applications, PANI has been functionalized with a wide range of materials, including: functionalized graphene nanosheets [14], reduced GO [15], carboxymethyl chitosan [16], chitin [17], phytic acid [18], sodium citrate-stabilized gold nanoparticles [19], starch [20], amino groups [21], nylon [22], amine-functionalized graphene [23], 3-aminobenzenesulfonic acid [24], nylon-66 [25], wool [26], PET [27], rayon [28], and polypropylene fibers [29]. Hu et al reported surface functionalization of PANI [30], while a facile method for preparing aminoacid-functionalized PANI was also described in the literature [31]. Additionally, iron-doped and dye-functionalized PANI was developed for supercapacitor applications [32]. Despite the variety of functionalization strategies reported, the literature reveals a gap—FC alkylation-based functionalization of PANI with enhanced electrical conductivity has not been extensively explored. The present research fills this gap, achieving high conductivity through this approach, marking the novelty of the current study.

FC reaction is a type of chemical reaction which attaches the substituents onto an aromatic rings in the presence of a catalyst such as $AlCl_3$ or $FeCl_3$. Alkylation and acylation are the two types of FC reaction. In 2010, Rueping et al reviewed the FC reaction [33]. FC polymerization leads to microporous polymer [34]. This type of material is useful for membrane application. FC reaction of alcohol with PEDOT conducting polymer was reported in the literature [35]. FC alkylation was done to increase the porosity of polymers [36]. In 2020, Suzuka et al reported the FC alkylation of indole under aerobic condition [37]. MWCNT was grafted onto PVC backbone via FC alkylation reaction [38]. FC-acylation reaction was supported with polymers [39]. FC reaction on PVC was thoroughly explained by Hace et al [40]. The phenylene based network polymer was synthesized by FC alkylation reaction [41]. Hyper branched polymers were synthesized via FC alkylation with high porosity [42]. Super adsorbent polymer was synthesized via FC alkylation reaction [43]. Cross linking of PS was done by FC reaction [44]. Hyper cross-linked polymer for CO_2 adsorption was carried out through FC alkylation reaction [45]. Recently, hyperbranched polymer with high porosity was synthesized via FC alkylation and acylation reaction [46]. Acid and amine functionalization was done on PI [47] and PSF [48]. In the present investigation also amine and acid functional groups were grafted onto PANI backbone via FC alkylation reaction towards improving the processability and electrical conductivity values. This is the novelty of the present research work.

2-methylimidazole (2MI) is a five membered heterocyclic water soluble hygroscopic white solid and used in the pharmaceutical dye industries as an intermediate chemical. 2MI has a pungent odour with the melting point of 145 ^{o}C. In 2MI, a methyl group is substituted in the second carbon atom. The unsubstituted imidazole is used in catalysis and polymer fields [49,50]. For eg. Copolymerization of imidazole with methylmethacrylate (MMA) [51] was reported in the literature. Copolymerization of imidazole with pyridine [52], N-vinyl pyrrolidone [53], benzothiazole [54] and methacrylicacid [55]. In 2018, Suyra [56] reported the N-vinyl imidazole grafted cellulose fiber. Controlled radical polymerization of 4-vinylimidazole was thoroughly studied and published [57]. Controlled polymerization of N-vinyl imidazole with dithiocarbamates towards high molar mass polymer was done by Haribabu et al [58]. In the case of 2MI, homopolymerization or copolymerization is restricted due to the presence of bulky methyl substituent. The main target of the present investigation is increase of solubility of PANI via Zwitter ion formation.

List of abbreviations

PANI-poly(aniline)
CEA-chloroethylamine
CAA-chloroaceticacid
PDS-peroxy disulphate
DDW-double distilled water
FC alkylation-Friedel-Crafts alkylation
FR-free radical
2MI-2-methylimidazole
$AlCl_3$-aluminumchloride
WCA-water contact angle
FTIR-fourier transform infrared
DSC-differential scanning calorimetry
TGA-thermogravimetric analysis
SEM-scanning electron microscopy
EDX spectrum-energy dispersive x-ray spectrum
ZOI-zone of inhibition
DTA-differential thermal analysis
ZP-zeta potential
SC-supercapacitor
PS-poly(styrene)
PSF-polysulfone
PI-polyimide
Aniline-ANI
RBF-round bottomed flask
NMP-N-methyl pyrrolidone

Materials and methods

Materials

Aniline (S.D. Fine chemicals, India, AR grade), potassium peroxydisulphate (PDS, CDH chemicals, India), HCl (Sigma Aldrich, India), *2*-methylimidazole (*2*MI, Merck chemicals, India) CEA (Sigma Aldrich, India), acetone, NMP, $AlCl_3$ and CAA were purchased from Sigma Aldrich, India were purchased and used as received. Double distilled water was used for solution preparation application. All chemicals used are hipure chemicals.

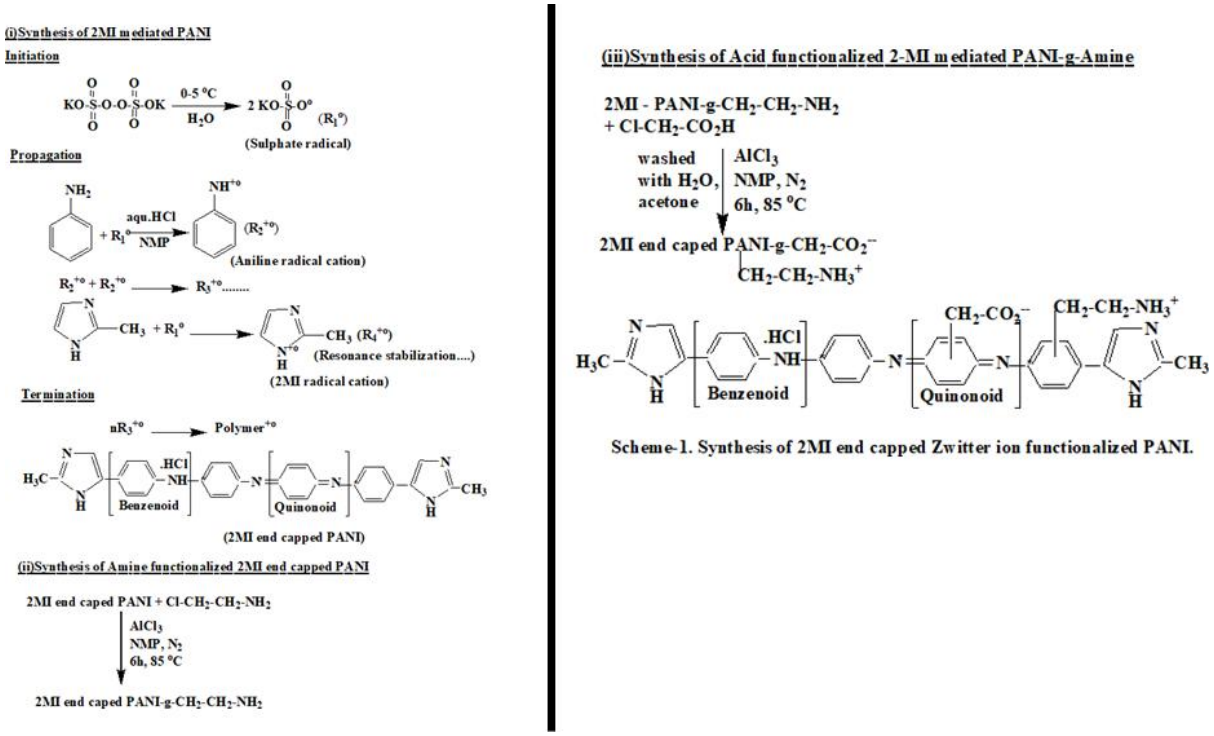
Synthesis of functionalized and end capped PANI

In this study, free radical (FR) solution polymerization of aniline (ANI) was carried out. A 1.0 M ANI solution was prepared using 1.0 M hydrochloric acid (HCl), and a separate 1.0 M aqueous solution of *2*-methylimidazole (*2*MI) was also prepared. Additionally, a 0.1 M solution of PDS was accurately prepared using double-distilled water (DDW). For the reaction, 10 mL of the 1.0 M ANI solution and 10 mL of the *2*MI solution were introduced into a 250 mL RBF equipped with a water-cooled condenser. The entire setup was placed in an ice bath maintained at 0–5 °C, and the mixture was stirred vigorously for 10 minutes under a nitrogen atmosphere. Subsequently, 20 mL of NMP and 10 mL of the PDS solution were slowly added while stirring continued for another 10 minutes. The formation of PANI was indicated by the appearance of a pale green color. Stirring was maintained for an additional 4 hours under continuous nitrogen purging to ensure complete polymerization. Upon completion, 250 mL of excess acetone was added to precipitate the *2*MI end-capped PANI. The precipitate was collected by filtration using a G4 sintered glass crucible and dried overnight at 60 °C. This sample was designated as A1.

The corresponding reaction scheme is presented in Scheme 1. The synthesis method was adapted from a standard literature procedure for end-capped PANI [59].

To prepare CEA-functionalized PANI, 1.0 g of *2*MI end-capped PANI and 0.50 g of CEA were dissolved in 25 mL of NMP. The mixture was stirred for 10 minutes to ensure complete dissolution. Subsequently, 0.10 g of $AlCl_3$ was added under a nitrogen atmosphere. This initiated the FC alkylation reaction [60], which was allowed to proceed at 85 °C for 6 hours. Upon completion, 250 mL of acetone was added to precipitate the product. The resulting CEA-grafted, *2*MI end-capped PANI was filtered and dried at 80 °C overnight. The dried sample was designated as A2 and stored in a zip-lock bag. The corresponding reaction pathway is illustrated in Scheme 1.

For the synthesis of acid-functionalized PANI, 1.0 g of the A2 sample was dissolved in 20 mL of NMP. To this, 0.50 g of CAA was added under a nitrogen atmosphere, followed by the addition of 0.10 g of $AlCl_3$. The mixture was stirred vigorously at 85 °C for 6 hours to carry out the FC alkylation reaction [60]. After the reaction, 500 mL of water was added to promote the formation of zwitterionic structures. Then, 300 mL of acetone was added to induce precipitation. The resulting solid was filtered using a G4 sintered glass crucible and dried at 60 °C overnight. This final product was labelled as sample A3 and stored in a zip-lock bag for further use. The complete reaction sequence is depicted in Scheme 1. PANI is a copolymer of amino and imino forms. During the amino functionalization via FC-alkylation reaction (considered as a first grafting), the amino group is grafted on to the benzenoid structure of PANI. Since it is a steric effect free, highly resonance and easy grafting cite. During the acid functionalization via FC-alkylation reaction (considered as a second grafting), the benzenoid structure may not be available for further grafting. If it is available, the chain length of CEA leads to steric effect. At this moment, the authors don't have any quantifiable data for first and second grafting processes. Hence, the FC-alkylation reaction preferred the quinonoid structure. Here no steric effect but needs high energy for further grafting. Sometimes, after first grafting, few reaction cite may be available in the benzenoid structure of PANI. The detail of the reaction is given in Scheme-1.



Scheme-1. Synthesis of 2MI end capped Zwitter ion functionalized PANI.

Scheme-1. Synthesis of 2MI mediated Zwitter ion functionalized PANI.

Characterizations

The polymer samples were characterized using various analytical techniques. UV–visible spectra were recorded using a Shimadzu 3600 NIR spectrophotometer (Japan) in the wavelength range of 200–800 nm, with NMP as the solvent. Thermogravimetric analysis (TGA) was performed on a Universal V4.4A thermal analyzer (TA Instruments, USA) under air atmosphere at a heating rate of 10 K min^{-1}. Fourier-transform infrared (FT-IR) spectra in transmission mode were obtained using a Shimadzu-8400 S spectrometer (Japan) in the range of 400–4000 cm^{-1}. Differential scanning calorimetry (DSC) was conducted on the same TA Instruments system under a nitrogen atmosphere, also at a heating rate of 10 K min^{-1}. Scanning electron microscopy (SEM) along with energy-dispersive X-ray spectroscopy (EDX) was performed using a JEOL 6300 instrument (USA) after gold coating the samples under vacuum. Water contact angle (WCA) measurements were carried out using a Kyowa DMs-200 goniometer (Japan), with the average value calculated from six different measurement points. Electrical conductivity was measured using a Keithley-617 four-point probe meter.

Determination of antimicrobial activity

The antibacterial and antifungal activities of the polymer samples were assessed using the spread plate method, employing various membrane components. At a fixed concentration of 15 mg, the membrane materials demonstrated antibacterial activity against *Escherichia coli* (*E. coli*). The observed antimicrobial properties of the membrane materials are attributed to the presence of C=N like structures in PANI and *2*MI [60].

Solubility test

Approximately 0.01 g of the polymer sample was placed in a 15 mL test tube. To this, 2 mL of NMP or other solvents (including water) were added separately. The polymer sample and solvent mixtures were thoroughly shaken and gently heated if necessary to aid dissolution. The solubility behavior of the sample was observed and is influenced by the chemical structure of the polymer.

Determination of % yield

The present investigation includes a three step reaction. Hence, the % yield at each step should be calculated by using the following formula:

$$\%\ yield = \frac{Weight\ of\ modified\ polymer\ obtained}{Weight\ of\ (polymer + modifying\ agent)}\ X\ 100 \quad \ldots \text{Eqn. (1)}$$

Results and discussion

% yield

In any chemical reaction, determination of % yield is very important. The % yield of A1 sample was calculated from Eqn. (1) as 99.8%. Sample A1 on structural modification with amine compound yielded the sample A2 as 95%. Sample A2 on structural modification with acid yielded the sample A3 as 81%. This low % yield is due to the FC alkylation reaction (i.e.) most of the reactive sites present on the aromatic benzene rings of PANI are completely occupied by amine grafting process. It means less reactive sites are freely available for the further acid functionalization process.

FTIR spectral study

Fig. 1a presents the FTIR spectrum of the A1 sample. Characteristic benzenoid and quinonoid ring stretchings of PANI were observed at 1477 cm^{-1} and 1566 cm^{-1}, respectively [59]. Stretching vibrations corresponding to C–N and C–N–C bonds were identified at 1379 cm^{-1} and 1122 cm^{-1}, [61,62] respectively. Aromatic ring vibrations appeared at 808 cm^{-1} and 599 cm^{-1}, while the Cl^- ion stretching was detected at 505 cm^{-1}. Notably, the absence of –NH or –OH stretching bands indicates that there are no free amino groups present in the sample. On close analysis one can see that the benzenoid peak at 1477 cm^{-1} is a doublet one. A peak at 1453 cm^{-1} is due to the skeleton vibration of 2MI ring. Here the peak intensity is very low because of low feeding of 2MI during the *insitu* polymerization. A small hump at 648 cm^{-1} is due to the bending vibration of 2MI ring [63]. Appearance of these two peaks confirmed the inclusion of 2MI in the PANI backbone. Fig. 1b shows the FTIR spectrum of the A2 sample. Along with the characteristic peaks observed in A1, several new peaks emerged. A broad band at 3381 cm^{-1} corresponds to the $–NH_2$ stretching vibration, attributed to the amino group of CEA. Additionally, a peak at 3194 cm^{-1} is associated with –OH stretching from physi-sorbed water molecules. Symmetric and asymmetric C–H stretching vibrations were identified at 2973 cm^{-1} and 3056 cm^{-1}, respectively. Fig. 1c displays the FTIR spectrum of the A3 sample, which retains the previously observed characteristic peaks. Two notable new peaks were detected: a strong band at 1725 cm^{-1}, corresponding to the C=O stretching of the CAA group [64], and a small hump at 1640 cm^{-1}, indicative of the formation of a zwitterionic structure resulting from interactions between amine and acid functional groups. This peak confirms the successful formation of a Zwitterion-functionalized, *2*MI end-capped PANI structure.

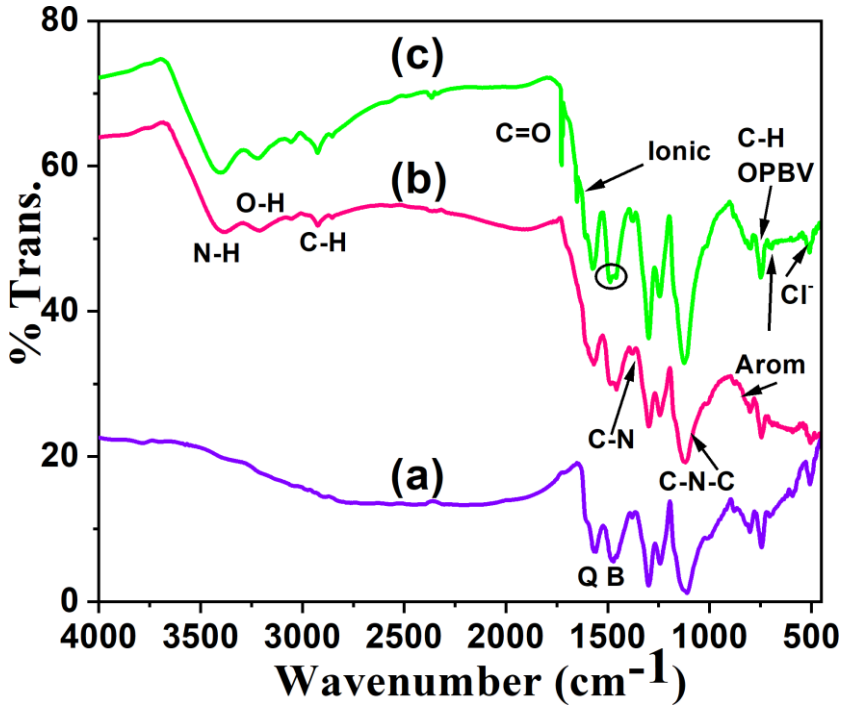


Fig. 1 FT-IR spectrum of (**a**)A1 system, (**b**)A2 system, (**c**)A3 system.

UV-visible spectral and bandgap studies

Fig. 2 presents the UV–visible spectra of the functionalized PANI samples. Fig. 2a corresponds to the A1 system, where absorption bands at 305 nm and 359 nm are attributed to π⟶π* and n⟶π* electronic transitions, respectively. A broad absorption peak observed at 652 nm is characteristic of the delocalized electronic structure associated with the conducting form of PANI [65]. Fig. 2b and 2c, corresponding to the A2 and A3 systems, also display these characteristic peaks, confirming the presence of HCl-doped PANI. In addition, both the amine- and acid-functionalized PANI samples exhibit four additional absorption peaks at 272, 308, 351, and 400 nm. These are attributed to π⟶π* transitions, n⟶π* transitions, the leuco-emeraldine structure of PANI, and extended conjugation of C=C double bonds, respectively. Overall, the UV–visible spectral data confirm the presence of various electronic transitions within the PANI backbone, indicative of successful functionalization and preserved electronic structure.

In order to find out the influence of grafting on the electrical conductivity value of PANI, the direct band gap value was determined from its UV-visible spectra. The band gap plot of 2MI incorporated PANI is given in Fig. 2d with the band gap value of 2.25 eV (Table-1). This confirmed the semiconducting nature of PANI. After the first grafting, the band gap value was increased to 2.95 eV (Fig. 2e, Table-1) again confirmed the semiconducting nature of PANI. After the second grafting process, still the band gap value rose to 3.05 eV (Fig 2f, Table-1). Anyhow, it is inside the semiconductor range. On comparison, one can say that while increasing the number of grafting process, the band gap value is slowly increased. This should decrease the electrical conductivity value of functionalized PANI. But, instead of decreasing the electrical conductivity, the electrical conductivity value was increased. This can be explained on the basis of interaction between NH_3^+ and CO_2^- ions. Formation of ionic structure was evidenced by the FTIR spectra (at 1640 cm^{-1}) (i.e.) formation of Zwitter ionic structure. Thus, the band gap value co-supported the FTIR spectrum. This result can be further supported by conductivity measurements data.

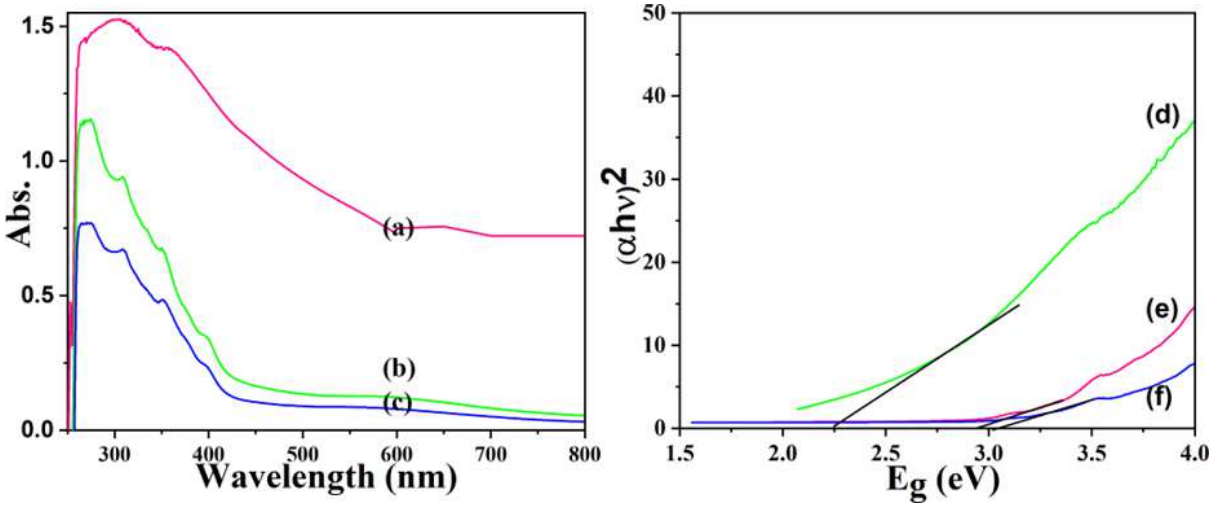


Fig. 2 UV-visible spectrum of (**a**)A1 system, (**b**)A2 system, (**c**)A3 system. Band gap plot of (**d**)A1 system, (**e**)A2 system and (**f**)A3 system.

Thermal studies

The DSC thermograms of the polymer samples are shown in Fig. 3. Fig. 3a illustrates the thermogram of *2*MI end-capped PANI (sample A1), displaying a glass transition temperature (T_g) at 65.4 °C. Although this temperature is sometimes associated with moisture loss or water loss, the step-like feature of the thermogram in this case suggests it corresponds to the T_g of PANI [66]. Following functionalization, the T_g values of the amine- (Fig. 3b) and acid-functionalized (Fig. 3c) PANI samples were determined and are summarized in Table 1. A slight increase in T_g was observed in both cases, attributed to the formation of zwitterionic structures within the polymer matrix. Among the functionalized samples, the amine-functionalized PANI exhibited the highest T_g value, likely due to the presence of inter- and intramolecular hydrogen bonding, which enhances thermal stability.

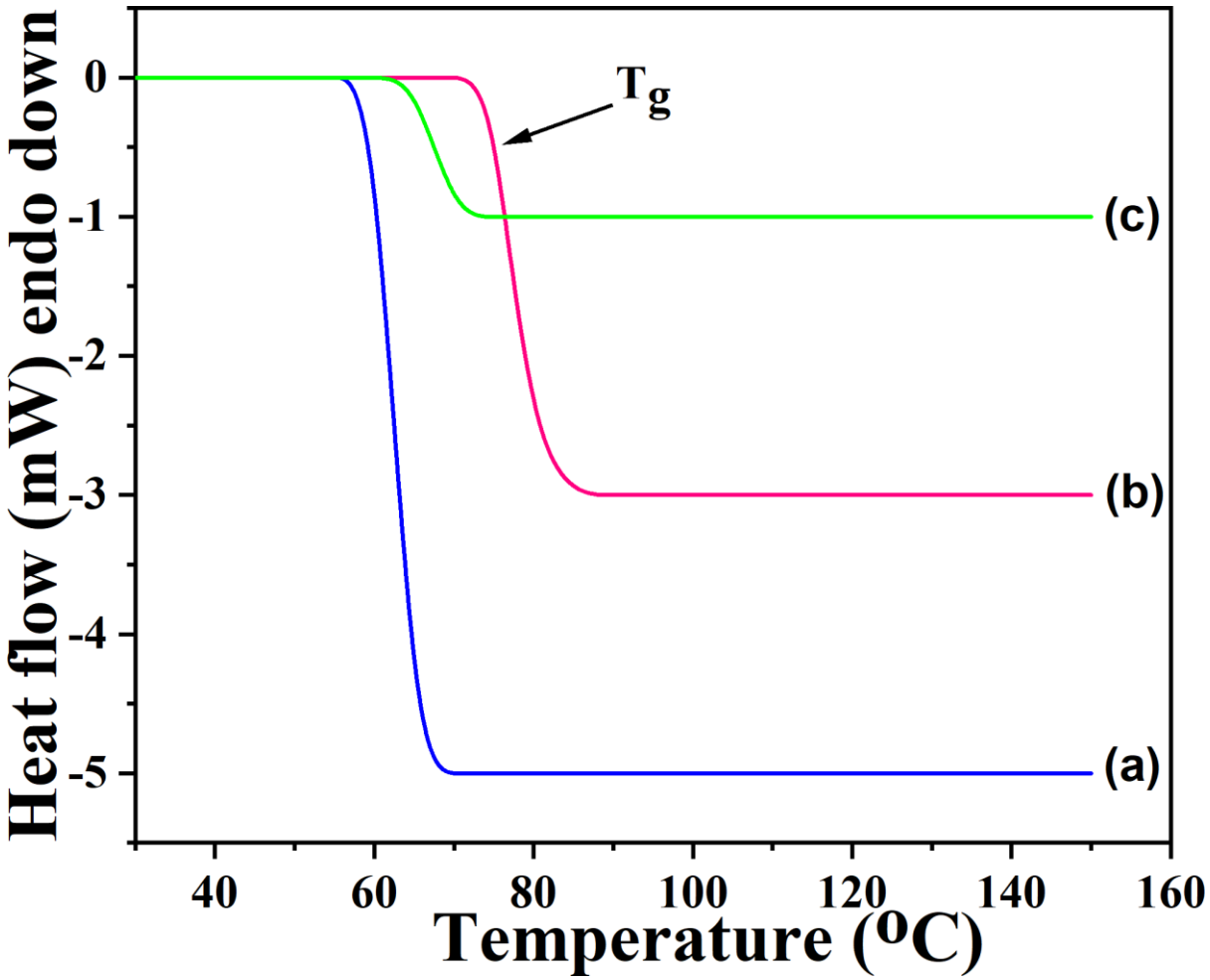


Fig. 3 DSC heating scan of (**a**)A1, (**b**)A2, (**c**)A3 systems.

Table-1
Thermal, Conductivity, ZP and WCA data

System	Code	WCA (°)	T_g (°C)	T_d (°C)	Conductivity (S/cm)	ZP (mV)	BG (eV)
PANI	A1	89.2	65.4	364	21.1×10^{-2}	25.5	2.25
PANI-g-amine	A2	65.6	73.1	403	38.5×10^{-3}	32.7	2.95
PANI-g-amine+acid	A3	61.4	67.7	417	10.4×10^{-1}	-1.3	3.05

The TGA thermograms of the polymer samples are presented in Fig. 4. Fig. 4a shows the thermogram of *2*MI end-capped PANI, which exhibits a two-step degradation process. The initial weight loss of approximately 20% observed below 100 °C is attributed to the evaporation of moisture and the removal of physi-sorbed water molecules. A significant weight loss occurs at 373 °C, corresponding to the thermal degradation of the PANI backbone. Above 750 °C, the system showed 3.1% weight residue remained. Compared to previous literature reports [67], the current system demonstrates an enhanced thermal decomposition temperature (T_d), likely due to the stabilizing effect of *2*MI end-capping. Fig. 4b displays the TGA thermogram of the amine-functionalized *2*MI end-capped PANI, which also follows a two-step degradation profile, similar to the A1 sample. The thermal data for all samples are summarized in Table 1.

The present system exhibited 5.4% weight residue remained above 750 ºC. Fig. 4c shows the TGA thermogram of the acid-functionalized PANI, which also exhibits a two-step degradation process. A major degradation event is observed at 420 °C, while a secondary degradation step appears at 610 °C, attributed to the decomposition of the –COOH-functionalized imino group in PANI, accompanied by the release of CO_2. 9.8% weight residue is remained above 750 ºC. On comparison of char remained above 750 ºC, the acid functionalized system showed ~10%. The high char formation may be associated with the formation of Zwitter ionic structure and intra and inter molecular hydrogen bonding increased the thermal stability of polymer sample. AS a result, the char formation is increased. The TGA analysis confirms that the amine-functionalized *2*MI end-capped PANI exhibits superior thermal stability, likely due to the formation of both intra- and intermolecular hydrogen bonds. Complementary differential thermal analysis (DTA) data for the *2*MI end-capped PANI and its amine- and acid-functionalized derivatives are shown in Fig. 5a–c, which further support the TGA findings.

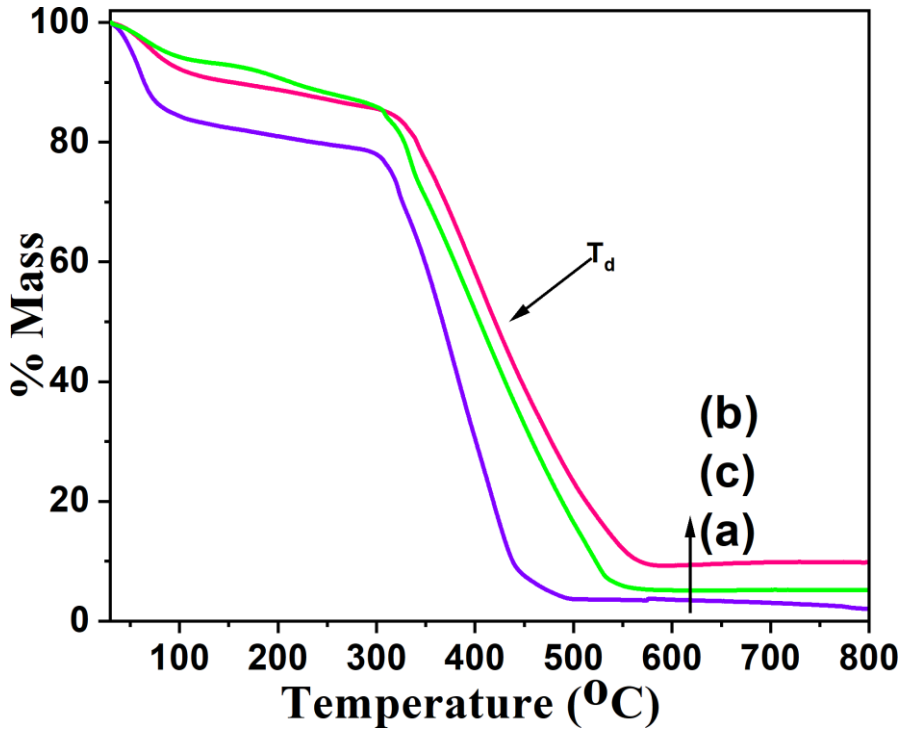


Fig. 4 TGA thermogram of (a)A1 system, (**b**)A2 system, (**c**)A3 system.

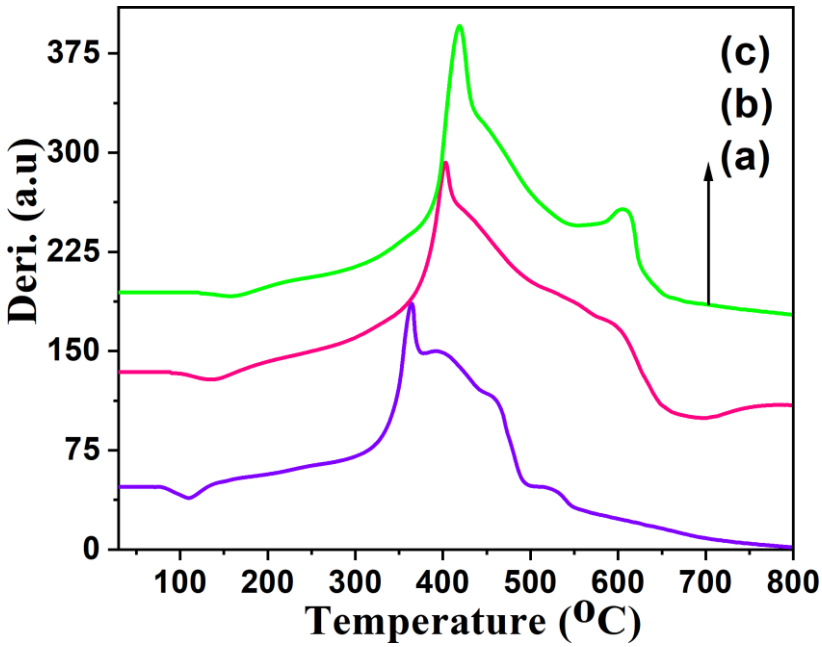


Fig. 5 DTA thermogram of (**a**)A1 system, (**b**)A2 system, (**c**)A3 system.

Antimicrobial study

The primary objective of the present study is to demonstrate the antimicrobial properties of PANI and its functionalized derivatives. A fixed amount of 15 mg of each sample was tested for both antibacterial (Fig. 6a–c) and antifungal (Fig. 6d–f) activities. All three samples exhibited notable antimicrobial and antifungal effects, which are attributed to the presence of C=N like structures in both the PANI backbone and the *2*MI units [68]. Among the samples, the acid-functionalized PANI demonstrated the highest activity, likely due to its enhanced solubility in aqueous media. *Escherichia coli* (*E. coli*) was used as the model organism for antibacterial testing. The presence of C=N like bonds—contributed by the rigid segments of PANI and the flexible *2*MI units—is believed to be a key factor in the antimicrobial efficacy of these systems. Fig. 6 d-f confirmed the anti-fungus activity of various functionalized polymer systems. Among the systems considered, the A3 system exhibited an excellent anti-fungus activity because of presence of zwitter ionic structure.

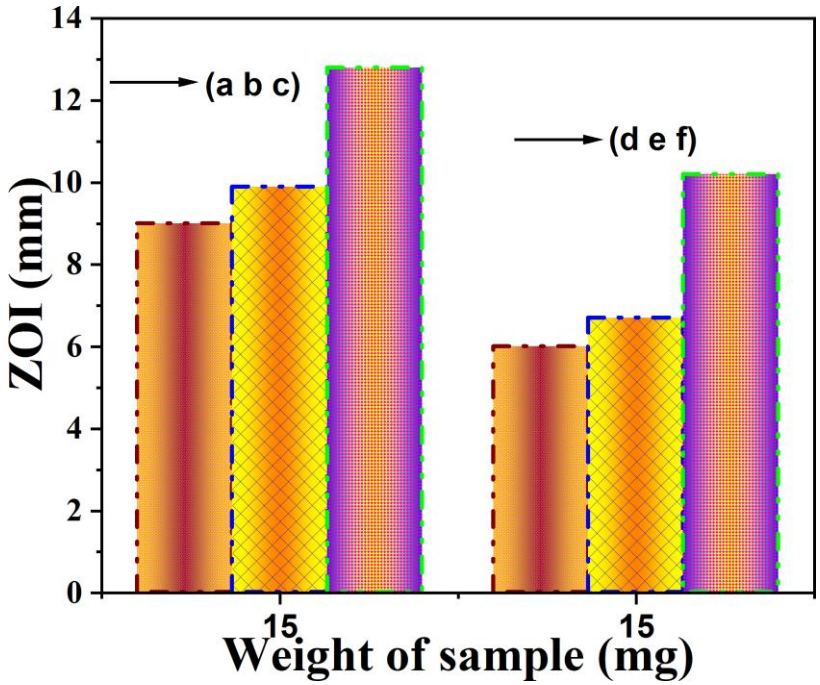


Fig. 6 Antibacterial activity of (**a**)A1 system, (**b**)A2 system, (**c**)A3 systems and anti-fungus activity of (**d**)A1 system, (**e**)A2 system, (**f**)A3 system.

WCA approach

The WCA measurements revealed significant variation due to amine and acid functionalization. The 2MI end-capped PANI displayed a WCA of 89.2°, while the amine- and acid-functionalized systems showed reduced WCAs of 65.6° and 61.4°, respectively (Fig. 7a–c; Table 1). Among the three, the acid-functionalized PANI exhibited the lowest WCA, indicating enhanced hydrophilicity. This increased hydrophilic nature is attributed to the zwitterionic character introduced through acid functionalization process. The WCA of f-PANI was reported as 75.78°. When compared with the literature value, the present system yielded lower WCA and confirmed the increase in hydrophilicity [69].

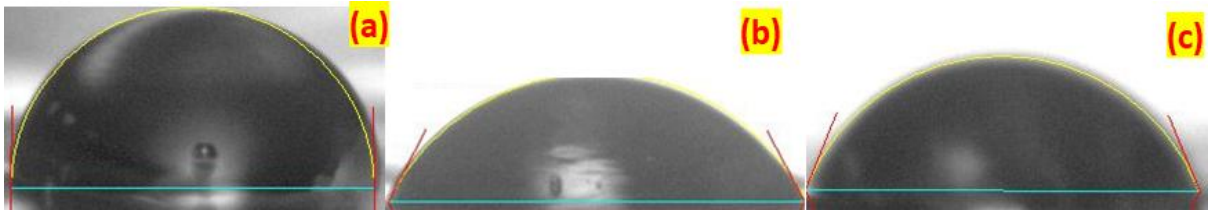


Fig. 7. WCA image of (**a**)A1 system, (**b**)A2 system, (**c**)A3 system.

Conductivity study

Table 1 summarizes the electrical conductivity values of all the systems studied. Among the three, the acid-functionalized 2MI end-capped PANI exhibited the highest conductivity, measured at 1.04 S/cm (10.4×10^{-1} S/cm), which aligns well with reported literature values [70]. This enhanced conductivity is attributed to the doping of the imine nitrogen atoms in the PANI backbone by HCl, as well as the presence of zwitterionic structures that facilitate charge transport.

Solubility study

In the present study, PANI was end-capped with 2MI and further functionalized with acid and amine groups. The solubility of the resulting polymers was evaluated in various solvents,

including water, NMP, DMSO, and DMF (Table 2). The samples exhibited moderate solubility in water and excellent solubility in NMP. This enhanced solubility, particularly in NMP, is attributed to the formation of intermolecular hydrogen bonding between the solvent molecules and the functional groups present in the polymer chains.

Table-2
Solubility test data

System	Solvents			
	Water	NMP	DMSO	DMF
PANI	++	+++	+++	++
PANI-g-amine	++	+++	+++	++
PANI-g-amine+acid	++	+++	++	++

Mechanism
It is well established that PANI can be synthesized via oxidative free radical polymerization, typically initiated using oxidizing agent such as PDS. Although polymerization of 2MI has not been reported in the literature, it is known to undergo co-polymerization at elevated temperatures. In the present study, polymerization was carried out at a low temperature range of 0–5 °C. This low-temperature condition favours the exothermic polymerization of ANI while simultaneously suppressing the co-polymerization of 2MI. As a result, the final product obtained is HCl-doped PANI end-capped with 2MI. To enhance the water solubility of PANI, both amine and acid groups were grafted onto the polymer backbone via the FC- alkylation reaction. It was observed that the rate of amine grafting was faster than that of acid grafting [60] suggesting that the amine groups preferentially attached to the benzenoid rings of the PANI backbone during the initial grafting stage. During the subsequent acid grafting step, most of the available benzenoid sites were already occupied, leaving the quinonoid structures as the primary reactive sites. Furthermore, the acid grafting reaction using CAA proceeded at a slower rate. However, the use of excess PDS facilitated secondary grafting of acid groups onto the quinonoid units of PANI. Thus, the present research effectively integrates oxidative FR polymerization and FC-alkylation to synthesize water-processable, functionalized PANI with improved solubility and conductivity.

Zeta potential report
The presence of ionic charges on the PANI backbone influences its ZP values. Under strongly acidic conditions (pH ~1.5), the abundance of H^+ ions resulting in positive ZP values [65]. As shown in Table 1, the 2MI end-capped PANI exhibited a ZP of +25.5 mV. Following amine grafting, the density of positive charges on the polymer surface increased, leading to a rise in ZP to +32.7 mV. In contrast, acid grafting introduced additional negative charges, causing the ZP to decrease significantly to –1.3 mV.

SEM analysis
The surface morphology of the 2MI end-capped PANI is shown in Fig. 8a, displaying a petal-like structure resembling plant petals, as highlighted by the yellow circle. Within this region, one or two microparticles smaller than 1 μm in diameter are visible. Fig. 8b presents the SEM image of the amine-grafted PANI, which exhibits a broken stone-like morphology. The yellow circle again highlights the presence of microparticles under 1 μm in size. Similarly, Fig. 8c shows the SEM image of the acid-grafted PANI, which also demonstrates a broken stone-like

surface texture. These observations suggest that despite undergoing one or two functionalization steps, the overall surface morphology of the PANI backbone remains largely unchanged.

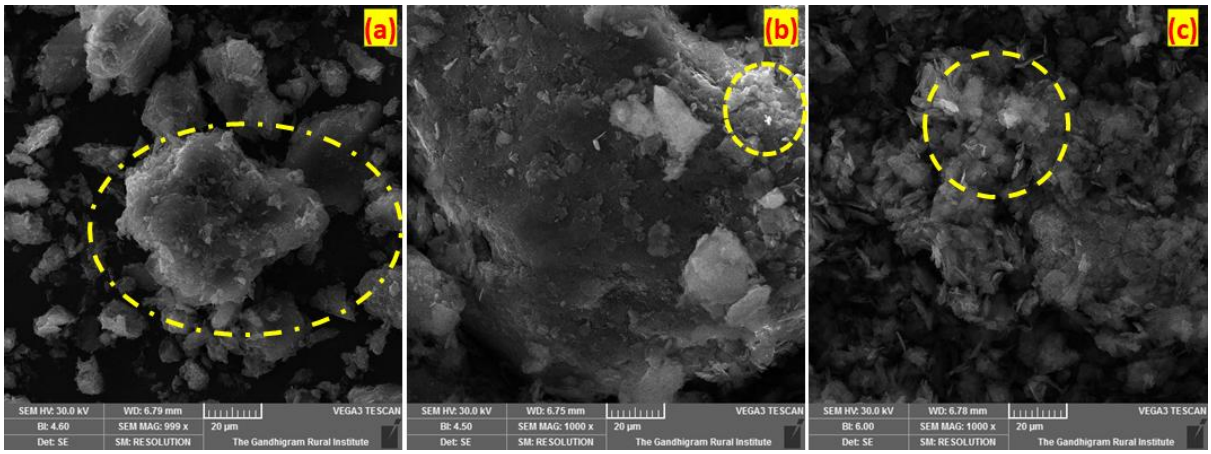


Fig. 8 SEM image of (**a**)A1 system, (**b**)A2 system, (**c**)A3 system.

EDX report

The elemental composition of the samples was confirmed through energy-dispersive X-ray spectroscopy (EDX). Fig. 9a shows the EDX spectrum of the *2*MI end-capped PANI, revealing the presence of carbon (73.8%), nitrogen (18.6%), oxygen (2.4%), and chlorine (5.2%). The carbon and nitrogen signals are primarily attributed to the PANI backbone, while additional nitrogen originates from the *2*MI end-capping unit. The presence of chlorine confirms doping with HCl, and the oxygen is attributed to physi-sorbed water molecules, as also supported by the TGA thermogram. The elevated nitrogen content indicates successful incorporation of nitrogen-containing moieties. These results are consistent with previous EDX studies reported in the literature [71]. Fig. 9b presents the EDX spectrum of the amine-grafted PANI, showing elements C, N, O, and Cl. A noticeable increase in nitrogen content further confirmed the successful grafting of CEA onto the PANI backbone. Fig. 9c displays the EDX spectrum of the acid-grafted, *2*MI end-capped, and amine-functionalized PANI. The spectrum shows C, N, O, and Cl, with an increase in oxygen content, which supports the successful grafting of CAA onto the polymer backbone. Overall, the EDX analysis clearly confirmed the chemical grafting of both amine and acid functional groups onto the PANI structure via the FC- alkylation reaction.

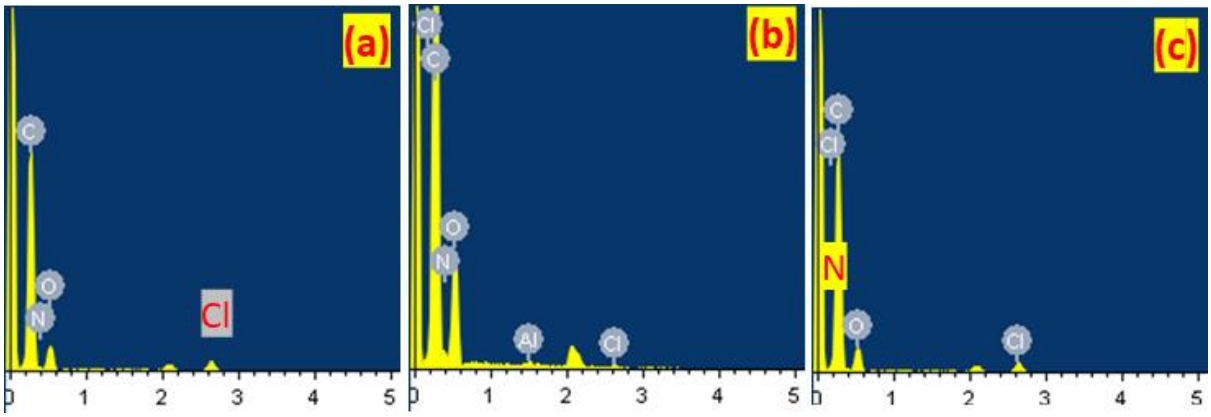


Fig. 9 EDX spectrum of (**a**)A1 system, (**b**)A2 system, (**c**)A3 system.

Conclusions

PANI was successfully synthesized via solution polymerization, with *2*-methylimidazole (*2*MI) employed as a chain end-capping agent. The A3 system produced low % yield because of less availability of active cites for FC alkylation reaction. FTIR analysis confirmed the formation of a zwitterionic structure, evidenced by the characteristic peak at 1640 cm^{-1}. UV–visible spectroscopy revealed an absorption peak at 652 nm, indicating the presence of the electrically conducting form of PANI. Among the synthesized systems, the amine-functionalized PANI exhibited the highest T_g of 73.1 °C. The WCA of the amine-functionalized sample (A2) was measured at 65.6°, while the acid-functionalized system (A3) demonstrated a ZP of –1.3 mV due to increased surface negative charge. Notably, the A3 sample also displayed the highest T_d of 417 °C and the highest electrical conductivity of 10.4×10^{-1} S/cm, attributed to the zwitterionic structure introduced through acid functionalization. In terms of biological activity, the A3 system showed superior antibacterial and antifungal performance, likely due to the presence of C=N like structures in both the PANI and *2*MI units. Additionally, the *2*MI end-capped PANI demonstrated good miscibility in water. SEM analysis confirmed the presence of microparticles, while EDX spectra revealed the elemental composition (C, N, O, and Cl) of all the samples. Overall, the combined strategy of end-capping and chemical grafting with both acid and amine groups significantly enhanced the chemical, thermal, and functional properties of PANI. These findings successfully fulfil the primary objective of the present research. Future work will focus on exploring membrane-based applications of the functionalized PANI systems.

Author contribution

A.Thamizhlarasan: Did all the experimental work and methodology, B.Meenarathi: Did all the analytical characterizations and formal analysis. A.Thamizhlthendral did the solubility test. R.Anbarasan: Wrote and review this research paper.

Declaration of Competing Interest

The authors declare no conflict of interest.

Financial support

There is no financial support for this piece of research work.

Data Availability

There is no data available.

References

1. Dube A, Malode S.J, Alodhayb A.N, Mondal K, Shetti N.P, (2025) Conducting polymer-based electrochemical sensors: Progress, challenges, and future perspectives. Talanta Open 11: 100395.
2. Lgaz H, Lee H.S, Alrashdi A.A, Messali M, (2026) Polyaniline based hybrid for corrosion protection: Breaking throughs in nanocomposite design, self-healing, and corrosion sensing. Polym Test 154: 109053.
3. Kishnani V, Makadia R.A, Natarajan S, Joseph J, Gupta A, (2025) Development of a silver-PANI functionalized bio-sensor for non-enzymatic lacticacid detection. Mater Adv 6: 766-776.
4. Wang L, Li C, Wang R, Lin Y, Xiong K, Wang B, Hao C, (2023) The preparation and smart electrorheological behavior of MOF-Ti@PANI core-shell nanoparticles. J Mol Liq 376: 121373.

5. Tejwani A, Sankar U, Shrives K, Pervez S, (2025) Differential pulse voltametric determination of dopamine using PANI functionalized grapheneoxide/silica nanocomposite for point of care diagnostics. RSC Adv 15: 15870-15878.
6. Sapudi M, Zaidi B, Alasime M, Ajjel R, (2021) PANI: Doping and functionalization with SWCNT for photovoltaic and photocatalytic application. Polymers 13: (2021) 2595.
7. Acevedo D.A, Salavagione H.J, Barbero C.A, (2005) Synthesis, properties and applications of functionalized PANIs. J Braz Chem Soc 16: 259-269.
8. Galloni M.G, Pina C.D, Bortolotto, V, Bianchi C.L, (2025) Highly porous PANI: a novel green catalytic method for morphology control. J Mater Sci 60: 5300-5325.
9. Park D, Lee D, Kim H.J, Hwang K.S, (2022) Scalable functionalization of PANI grafted GO field effect transistors for a highly sensitive enzymatic acetycholine biosensor. Biosensors 12: 279.
10. Badry R, Elhaes H, Ibrahim A, Ibrahim M.A, (2024) Investigating the electronic properties and reaction of PANI emeraldine base functionalized with metal oxides. Sci Rep 34: 27024.
11. Cardaso R, Lima S, Lenz M, (2007) PANI synthesized with functionalized sulfonicacids for blends manufacture. Mater Res 10: 425-429.
12. Nikolaidis G, Stanisavljev R, Zunovic D, (2010) Microwave assisted synthesis of functionalized PANI nanostructures with advanced anti-oxidant properties. J Phys Chem C 114: 18790-18796.
13. Tritscher F, Mularcyzk A, Cuenca A.F, Bodner M, (2023) Surface doped PANI coating for functionalized gas diffusion layers in low temperature fuel cells. Mater Adv 4: 2573-2585.
14. Altin Y, Unsal F, Bedeloglu C, (2021) Fabrication and characterization of PANI functionalized graphene nanosheets/PDMS nanocomposite films. Polym Polym Compos 29: 5741-5752.
15. Verma D.K, Prajapati S, Sahu M, Rastogi R.B, (2024) Super lubricity of nanocomposites of PANI functionalized reduced grapheneoxide with Yttrium and vanadium co-doped ZnO composites. ACS Appl Eng Mater 2: 156-169.
16. Solimani S.A, Irani A, (2023) Carboxymethyl chitosan functionalized PANI/ Poly(acrylonitrile) nano fibers for neural differentiation of mesmenchymal stem cells. Appl Biochem Biotechnol 195: 7638-7651.
17. Ayed E.B, Ghorbel N, Boufi S, (2023) PANI grafted chitin nanocomposites and conductive reinforcing nanofillers for waterborne polymer dispersions. ACS Biomacromolecules 23: 4167-4178.
18. Yan B, Chen Z, Cai L, Xu Q, (2015) Fabrication of PANI hydrogel: synthesis, characterization and adsorption of methylene blue. Appl Surf Sci 356: 39-47.
19. Sanches E.A, Soares J.C, Marangoni V.S, Mascarenhas Y.P, (2011) Structural characterization of emeraldine solid PANI/Au nanoparticle complexes. J Nanomater 2011: 697071.
20. Boudjelida S, Li X, Carraro M, (2024) Synthesis and characterization of PANI emeraldine salt colloids using potato starch as a stabilizer to enhance the physico-chemical properties and processabilities. Materials 17: 2941.
21. Joseph A, Subramanian S, Ramamoorthy P.C, Sampath S, Schwandt C, (2015) Amine functionalized PANI grafted to exfoliated graphite oxide. Synthesis, characterization and multi-element sensor studies. J Electroanal Chem 757: 137-143.
22. Thornton E, Harrison A, Pharm L. Castano E, C. Tang C, (2018) PANI functionalized new fibers for calorimetric detection of HCl vapor. ACS Omega 3: 3587-3591.
23. Abdali H, Heli B, Ajji A, (2019) Stable and sensitive amino functionalized graphene/PANI nanofiber composites for room temperature CO_2 sensing. RSC Adv 9: 41240-41247.

24. Zhang L, Lang Q, Shi Z, (2010) Electrochemical synthesis of 3D PANI network on 3-aminobenene sulfonicacid functionalized glassy carbon electrode and its application. J Anal Chem 1: 102-112.
25. Anbarasan R, Vasudevan T, Gopalan A, (1998) Modification of nylon6 into conducting fiber by peroxosalts initiated graft copolymerization-A kinetic approach. Int J Polym Mater 42: 195-208.
26. Anbarasan R, Vasudevan T, Gopalan A, (1999) Characterization of chemical grafting of PANI onto wool fiber. Int J Polym Anal Charact 5: 247-256.
27. Anbarasan R, Vasudevan T, Gopalan A, (1999) Chemical grafting of aniline and toluidine onto PET fiber. J Appl Polym Sci 73: 121-128.
28. Anbarasan R, Nirmala P.V, Sudha M, Gopalan A, (2000) Peroxosalts initiated graft copolymerization of o-toluidine onto rayon fiber -A kinetic approach. Int J Polym Mater 48: 199-223.
29. Anbarasan R, Sudha M, Gopalan A, (2000) Peroxomonosulphate initiated graft copolymerization of aniline onto PP fiber – A kinetic approach. Compos Inter 7: 312-329.
30. Hu J, Li S.S, Li J.F, Wang Y.L, (2022) Surface functionalization of PANI and electrocatalytic performance for oxygen reduction to produce H_2O_2. Chem Eng J 431: 133921.
31. Anbarasan R, Gopalan A, (2000) Peroxosalts initiated graft copolymerization of aniline onto wool fibre—a comparative: kinetic study. J Mater Sci 35: 617-625.
32. Yazar S, Besir M, Sahim Y, (2022) Hydrothermal synthesis of flexible Fe doped/dye functionalized carbon felt electrode for super capacitance application. Chem Sel 7: e202200016.
33. Rueping M, Nachtsheim B.J, (2010) A review on new development in the FC alkylation from green chemistry to asymmetric catalysis. Beilstein J Org Chem 6:1-24.
34. Krusenbaum A, Geisler J, Kraus L, Borchardt L, (2022) The mechano-chemical FC polymerization as a solvent tree cross linking approach toward microporous polymers. J Polym Sci 60: 62-71.
35. Angelo D, Kumar A, Onaro A, Smith B, (2007) Chemical stability of conducting polymer FC reaction of alcohols with poly(3,4-ethylediethoxythiophene) (PEDOT). Polymer 48: 4328-4336.
36. Troschke E, Gratz S, Lubkea T, Borchardt L, (2017) Mechanochemical FC alkylation. A sustainable pathway towards porous organic polymers. Angew Chem 129: 1-6.
37. Suzuka T, Ooshiro Y, Ogihara K, (2010) FC type alkylation of indoles in water using amphiphilic resin supported 1,10-phenonthroline-Pd complex under aerobic condition. Catalyst 10: 193.
38. Wu X.L, Wu L, Liu P, (2010) PVC-g-MWCNT via FC alkylation. Exp Polym Lett 4: 723-728.
39. Deshmuk A.P, Padiya K.J, Salunke M.M, (1999) FC alkylation reaction using polymer supported Aluminum chloride. J Chem Res 5: 568-569.
40. Rozyyev V, Hong Y, Yavuz S, Thirion D, Yavuz C.T, (2021) Extensive screening of solvent linked porous polymers through FC reaction for gas adsorption. Adv Eng Sust Res 2: 2100064.
41. Liu Z, Yang T, Song Y, Zhao N, (2026) Hyper cross linked polymer by an external cross linker strategy: formation of mechanistic, structural regulation and applications. RSC Appl Polym (in press).
42. Saeidian H, Moghaddan F.M, Soh A, (2009) Super adsorbent polymer as nanoreactors for preparation of hematite nanoparticles and application of the prepared nano catalyst for the FC acylation. J Braz Chem Soc 20: 466-471.
43. Yao H, Dick C, Liggat J.J, Shape C.E, (2001) Cross linking by FC chemistry. Reaction of p-hydroxy benzylchloride with polystyrene. Polym Degrad Stab 72:399.

44. Lau C.H, Lu T.D, Sun S.B, Chen X, Dawson D.M, (2019) Continuous flow knitting of a triptcene hyper crosslinked polymers. Chem Commun 55: 8479-8574.
45. Begni F, Gullo F, Ferrari M.C, (2022) Optimisation of the FC alkylation for the synthesis of crossed linked polymers. ACS Appl Polym Mater 4: 5281-5286.
46. Raubineau N.J, Castro E.C, Rane K, Fiese M.F, (2024) Understanding the competition between hydrodechlorination and FC alkylation in PVC dehydrochlorination with silylium ions. Polym Chem 16: 2514.
47. Duan Z.Y, Wang Y.Y, Pan Q.W, Chen Z.Y, (2022) Hyper cross linked polymers fabricated from divinylbenzene via CF addition polymerization. Chin J Polym Sci 40: 310-320.
48. Feng J.J, Wang M, Hu Y, Deng Z.T, (2017) Hyper cross linked polyporphyrin by metal free protocol: characterization uptake performance and heterogeneous catalysis. Design Monom Polym 20: 344-350.
49. Li L, Tian S, Xu E, Fei X, Dyson P.J, (2026) The versatility of imidazole and imidazolium scaffolds in sustainable chemistry and energy conversion. Helvet Chim Acta 109: e00188.
50. Yun Y, Xia W.T, Hu S, Li Q.H, Zhang J, (2026) Imidazole based MOFs for photo/electrocatalytic CO_2 conversion: controllable construction, mechanistic investigation, and machine learning. Ener Chem (in press).
51. Yildiz M, Alp S, Saltan F, Akat H, (2020) Synthesis of new imidazole based monomer and copolymerization studies with methylmethacrylate. Iran Polym J 29: 515-523.
52. Raj V, Madheswari D, Ali M.M, (2012) Chemical synthesis, characterization and properties of conducting copolymers of imidazole and pyridine. J Appl Polym Sci 124: 1649-1658.
53. Green M.D, Allen M.M, Dennis J.M, Long T.E, (2011) Tailoring macromolecular architecture with imidazole functionality: A perspective for controlled polymerization process. Eur Polym J 47: 486-496.
54. Bajer I.K, Nowakowski N, Drapola J, Wielgus I, Piconona K, (2022) Copolymers containing 1-methyl-2-phenyl imidazole moieties as permanent diole generating units: Synthesis, spectro-electrochemical and photo-voltoic properties. Molecules 27: 915.
55. Annenkov V, Tenhu H, Aseyev V, Hinvonen S.P, Mikhaleva A.I, (2004) Copolymers of 1-vinyl imine and methacrylicacid: synthesis and polydegradation properties. Eur Polym J 40: 1027-1032.
56. Surya S, (2018) Comparative study of grafting kinetics of N-vinyl imidazole and vinyl pyridine onto cellulose. Int J Theor Appl Sci 10: 222-233.
57. Allen M.H, S.T. Hemp S.T, Smith A.E, Long T.E, (2012) Controlled radical polymerization of 4-vinyl imidazole. Macromolecules 45: 3669-3676.
58. Haribabu P.M, Vijayakrishna K, (2024) Controlled polymerization of N-vinyl carbazole, N-vinyl pyrrolidone and N-vinyl carbazole with dithiocarbamates toward high molar mass polymers. Macromol Chem Phys 225: 24003871.
59. Anbarasan R, Kenet Nancy Mary M, Jancirani A, Baskaran R, (2024) Synthesis, characterization and thermal studies of NIR fluorescent probe based on poly(anthranilicacid)/ Sand nanocomposites. Polym Bull 81: 14083.
60. Anbarasan R, Amala Jeya Ranchani A, Tung K.L, (2022) Synthesis and characterization of Zwitter ion functionalized PSF membrane. Chem Sel 7: e202200406.
61. D Balakrishnan D, C. Pragathiswaran C, K. Thanikasalam K, Y. K. Mohanta Y.K, M. Saravanan M, M. H. Abdellattif M.H, (2022) Molecular docking and in vitro inhibitory effect of Polyaniline (PANI)/ZnO nanocomposite on the growth of struvite crystal: a step towards control of UTI. Appl Biochem Biotechnol 194: 4462-4476.
62. Reka Devi M, Joseph Sahaya Anand T, Muthuvinayagam M, Yogalakshmi K, M. Shaheer Akhtar M, (2024) Studies on optoelectronic properties of polyaniline/Zinc oxide *p–n*-heterojunction diode. J Nanoelect Optoelect 19: 1338-1346.

63. Mandana S, Razich F, Hamid A, (2016) Nanostructured sodium zeolite imidazolate framework (ZIF-8) doped with K by sol-gel processing for bio-diesel production from soy-bean oil. J Sol Gel Sci Technol 77: 404-414.
64. Kailash S, Meenarathi B, Anbarasan R, (2020) Conjugated hydrophobic and hydrophilic blocks through a drug moiety as a leading macromolecular system sustainable drug delivery. J Polym Res 27: 355.
65. Rafiq S, Lovely M.A, Mim S.R, Billah M.M, (2025) Structure controlled enhanced photo catalytic activity of polyaniline. Heliyon 11: e42888.
66. Conklin J.A, Huang S.C, Huang S.M, Wen T, Kaner R.B, (1995) Thermal properties of polyaniline and poly(aniline-co-o-ethylaniline). Macromolecules 28: 6522–6527.
67. Yelilarasi A, Jeyakumari J.J.L, Anbarasan R, (2009) FTIR spectroscopy: A useful tool for structural determination of polyaniline nanocomposites. Polym Polym Compos 17: 411-421.
68. Revathi N, Sankarganesh M, Dhaveed Raja J, Johnson Raja S, Jeyakumar T.C, (2023) Synthesis, spectral, DFT calculation, antimicrobial, antioxidant, DNA/BSA binding and molecular docking studies of bio-pharmacologically active pyrimidine appended Cu(II) and Zn(II) complexes. J Biomol Str Dynam 41: 14914-14928.
69. Falak S, Shin B.Y, Hug D.S, (2022) Antibacterial activity of PANI coated in the patterned film depending on the surface morphology and acidic dopant. Nanomaterials 12: 1085.
70. Kamarudin S, Rani A, Mohammad M, Razali H, (2021) Investigation on size and conductivity of polyaniline nanofiber synthesized by surfactant free polymerization. J Mater Res Technol 14: 255-261.
71. Manjunatha S, (2025) Polyaniline/$CoNiO_2$ nanocomposites: Synthesis, characterization and thermal study. Adv Mater Lett 16: 2501.